DX.DOI.ORG//10.19199/2023.168.1121-9041.05

Rockfall embankments. Innovative design and construction methods

Robert Hofmann*

* University of Innsbruck, Unit for Geotechnical Engineering

Corresponding author: robert.hofmann@uibk.ac.at

The Austrian standard ONR 24810, 2020 regulates the effects of actions, design, construction, monitoring and maintenance of rockfall protection embankments. This standard describes the design concept and the constructions in detail. The basic principles are based on the research results of Hofmann & Mölk, 2012, Hofmann et al., 2013, Hofmann et al., 2017 and Hofmann et al., 2020. The constructions are differentiated into five types depending on the front facing and the geosynthetic reinforcement (Table 2). Type I refers to embankments without geosynthetics. Embankments with a stone facing on the uphill side are type II. The constructions reinforced with geosynthetics represent the construction types III, IVa and IV b. The geosynthetic-reinforced embankments without increased transverse distribution of the impact loads is type III, the geosynthetic-reinforced embankments with increased transverse distribution is type IVa and with strongly increased transverse distribution is type IVb. This design concept is used e.g. in Austria, Switzerland, Germany, Italy and Norway.

Keywords: *Rockfall, embankments, Geotechnical verification, innovative constructions.*

1. Introduction

A static equivalent load estimated in the first step, based on the penetration depth of the boulder (block) into the embankments, forms the basis of the design concept according to Hofmann & Mölk, 2012. The penetration depth (point of impact) is determined with the help of dimensionless design diagrams (Fig. 8). Studies by various authors (e.g. Kretz, 2018 and Marchelli, *et al*., 2021) in recent years have consistently confirmed the order of magnitude of the penetration depths determined with the diagrams. Rheological models as described in Ronco *et al*., 2007 and Marchelli, *et al*., 2022, also represent a theoretically well justifiable procedure to prove sufficient dam geometry (depth of penetration of the block into the embankments and valley-side displacements). However, the determination of the appropriate material parameters (determination of the lateral friction forces, deformation modulus of the embankment, friction angle during impact loading, valley-side deflection in the area of the impact) is a challenging task that requires a lot of experience. The mass of the mobilized embankments cross-section can only be estimated. However, the determination of the penetration depth using the empirical formula of Montani (ASTRA, 2008), for the static equivalent force is to be considered critically for rockfall protection embankments. This formula is based on the free fall of a block onto a rockfall protection gallery and thus on a completely different model with a rigid layer below the fill. In the documented events at protective embankments in Switzerland, no downhill displacement of the dam surface was detected (Kretz, 2018). This finding is in contradiction to the rheological calculation model given. The assumptions for a design concept based on rheology requires an expert with a lot of experience. A determination of safety against failure is also not possible with this method. Another possibility for the design of rockfall protection embankments is the authors' proposal with a simple geotechnical model. Based on extensive model experiments (Hofmann & Mölk, 2012, Hofmann *et al*., 2017), a dimensionless diagram was developed for determining the penetration depth of the block depending on the different embankment's types. Based on the penetration depth, the kinematic basic equation is used to determine the static equivalent force. The applicability of the design concept has been used in recent years on various types of structures with validation calculations on documented events. The calculation method according to Ronco, *et al*. 2009 as well as Marchelli, *et al*. 2022 and the calculation concept presented here (Hofmann & Mölk, 2012, Hofmann *et al*., 2017 and Hofmann *et al*., 2020) should be used in parallel to make best use of the advantages of both methods. Figure 1 shows the energy ranges for the different protective structures. The protective embankments cover an energy in the range of 400 kJ to 30,000 kJ.

2. Design information for rockfall protection dams in Swiss regulations

Geometric recommendations for rockfall protection embankments according to Office for Forests of the Canton of Bern and the Federal Department of the Environment, Transport, Energy and Commu-

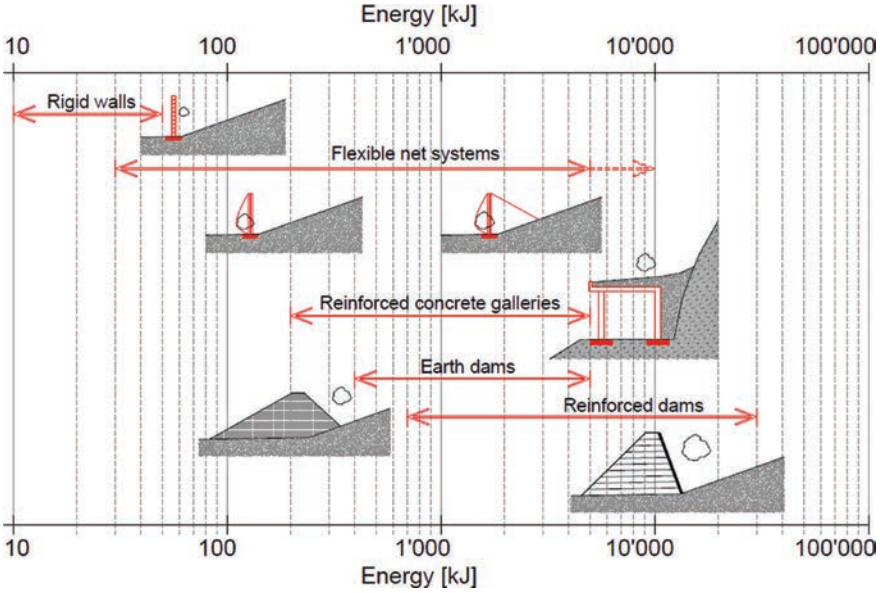

Fig. 1 – Energy ranges of protective structures.

nications, 2015 are summarised in Table 1. It is noticeable that no distinction is made between different types of construction, e.g. embankments without geosynthetics, embankments with stone facing and geosynthetics-reinforced embankments. The freeboard must be increased for reinforced embankments compared to embankments without geosynthetics. There are no instructions for the geotechnical design and verification (GEO) in this code.

The specifications in Kister & Fontana (2012), which were based on several research projects at the Lucerne University of Applied Sciences and Arts with small-scale quasi 2D experiments and half-scale 3D experiments, are very similar to the specifications in Office for Forests of the Canton of Bern and the Federal Department of the Environment, Transport, Energy and Communications, 2015. In model tests (Hofmann & Mölk, 2012 and Hofmann *et al*., 2017), the influence of block rotation was investigated and the need to consider it for the design and dimensioning of rockfall protection embankments was mentioned. From the model experiments, three geometric requirements (crown width, dam width at the point of impact and freeboard) could be derived for the rockfall protection embankments (Table 1). However, a design concept for the verification of the ultimate limit state ULS is not given here either. It should be noted that all model experiments were carried out with cohesive model soil with unrealistic slope inclinations for the large-scale design of up to 5:1, whereby no model geosynthetics were used in any of the experiments.

3. Construction types for rockfall protection embankments

The five construction types (I, II, III, IVa and IVb) differ in the front design and the arrangement of the geosynthetics in the dam body (Table 2). Pure earth dams are referred to as type I; in type II, the uphill slope is constructed with stone fillings (ONR 24810, 2020, Hofmann *et al*. 2017).

The embankments reinforced with geosynthetics can be assigned to type III, type IVa or IVb for the design of the rockfall event, depending on the tensile and strength of the reinforcement. In the case of

Tab. 1 – Geometric guidelines for rockfall embankments according to Office for Forests of the Canton of Bern and Federal Department of the Environment, Transport, Energy and Communications, 2015.

Geometric characteristic of the embankment	Minimum value according to Office for Forests of the Canton of Bern	Minimum value according to Federal Department of the Environment, Transport, Energy and Communications, 2015	Note
Crown width	1.0 D – 1.2 D	1,2 D	D (m) block diameter
width at the point of impact	2.5 D – 3.3 D	3 D	
width at point of impact for protective embankments with stone facing	-	2,5 D	
height	1.33 h_A – 1.5 h_A	-	h_A (m) jump height
Freeboard	0.5 D – 1.0 D	0,8D	For embankments with geosynthetics ≥ 1.0 D (m)
slope uphill side	≥ 60°	≥ 60°*)	*) independent of the embankments construction

Tab. 2 – Construction types.

Type	Definition
I	Embankment without geosynthetics (Fig. 2)
II	Embankment with a stone facing (Fig. 4)
III	Embankment with geosynthetic reinforcement to secure the slope, but without the additional requirements for geosynthetics for greater transverse distribution (Fig. 3).
IVa	Slender embankment reinforced with geosynthetics (Fig. 5), with a larger transverse distribution (6 to 7 times the block diameter) of the impact from the rockfall event (Table 3).
IVb	Slender embankment reinforced with geosynthetics (Fig. 5), with a larger transverse distribution (8 to 9 times the block diameter) of the impact from the rockfall event than in construction type IVa (minimum requirements for the geosynthetics according to Table 4).
S	Special types are combinations of embankment types I to IV

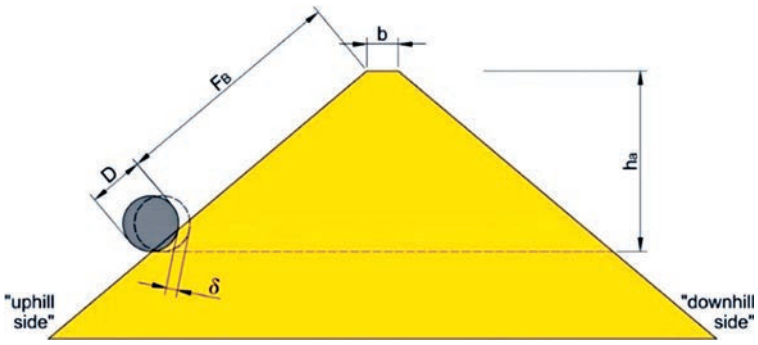

Fig. 2 – Type I.

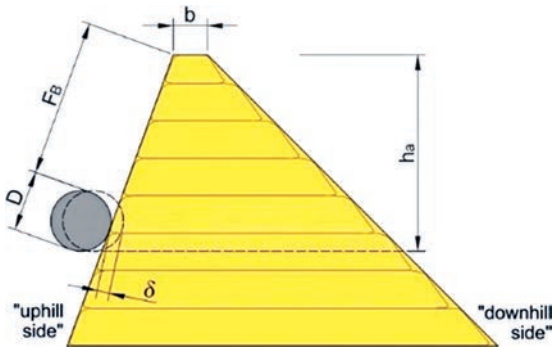

Fig. 3 – Type III.

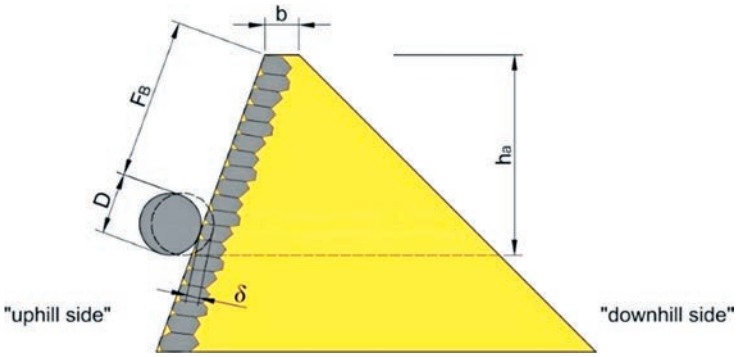

Fig. 4 – Type II.

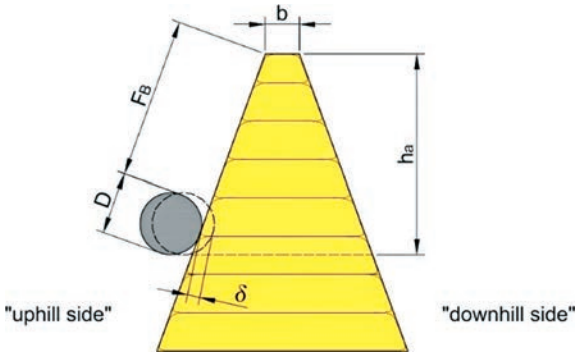

Fig. 5 – Type IVa/IVb.

Tab. 3 – Requirements for reinforcement with low tensile strength/elongational stiffness *Type IVa.*

Reinforcement	orientation relative the longitudinal axis of the dam	
	transverse	in the direction of the dam axis
Design strength $R_{B,d}$	≥ 110 kN/m	≥ 30 kN/m
Design value of elongation stiffness $J_{d@5\%}$	≥ 2200 kN/m	≥ 550 kN/m

Tab. 4 – Requirements for reinforcement with high tensile strength/elongational stiffness *Type IVb.*

Reinforcement	orientation relative the longitudinal axis of the dam	
	transverse	in the direction of the dam axis
Design strength $R_{B,d}$	≥ 225 kN/m	≥ 125 kN/m
Design value of elongation stiffness $J_{d@5\%}$	≥ 4500 kN/m	≥ 2500 kN/m

Tab. 5 – Recommendations for transverse distribution and freeboard.

Type	Transverse influence length x-times block diameter D	Freeboard x-times block diameter D
I	5-6	2,0
II	5-6	2.0/1.0 (with $\beta_B \geq 50°$)
III	5-6	1.5/1.0 (with $\beta_B \geq 70°$)
IVa	6-7	1.5/1.0 (with $\beta_B \geq 70°$)
IVb	8-9	1.5/1.0 (with $\beta_B \geq 70°$)

type III, requirements for geosynthetics are not given; the distribution of the static equivalent force from an impact event then corresponds to that of an embankment without geosynthetics (Type I).

In case the requirements are met, a significantly wider load distribution may be applied, which allows the dissipation of very large energies even in very slender constructions. The minimum requirements for the reinforcement can be distributed proportionally to the reinforcement layers depending on the selected layer spacing. The model experiments on a scale of 1:33 with different model geosynthetics and embankment construction materials are described in detail in Hofmann & Mölk, 2012, Hofmann *et al*., 2017 and Hofmann *et al*., 2020.

Type I *embankment without geosynthetics*

Depending on the shear strength of the embankment fill material, maximum slope inclinations of 2:3 to a maximum of 4:5 are possible. However, these slopes are unfavourable for the serviceability of the construction (safety against rolling over of the embankment) and therefore require a larger freeboard of at least 2 times the block diameter. The freeboard is defined as the distance from the top edge of the design block to the top of the embankment in the direction of the fall line of the uphill slope face. The "activated embankment body" at impact reaches a maximum width of about 5 to 6 times the design block diameter in the direction of the embankment axis.

Type II *embankment with stone facing*

In order to improve the load-bearing capacity and serviceability, the embankment can be constructed with stone facing on the uphill side. This measure leads to a reduction of the freeboard and at the same time to an increase of the load-bearing capacity in case of rockfall. The activated embankment body reaches a maximum width of 5 to 6 times the design block diameter. A freeboard of at least the single block diameter D is required for a slope inclination ≥ 50°. During impact, the boulder is enclosed by the blocks of the stone fill, which prevents the impact body from rolling up to the embankment crest.

Type III *embankment reinforcement with geosynthetics only for securing the slope inclination*

With geosynthetics, the embankments can be made steeper. However, these embankments are not to be designed according to the specifications for reinforced embankments of type IVa or IVb. *The* reinforcement with geosynthetics leads to an improvement of the serviceability with regard to the safety against "rolling over" of the embankment and thus a reduction of the freeboard can be achieved at certain minimum slope inclinations. A freeboard of at least 1.5 times the block diameter D is required. However, for constructions with an embankment slope of ≥ 70°, the freeboard can be reduced to the simple design block diameter D, as is the case for type IV. The activated dam body only reaches a maximum width of 5 to 6 times the block diameter.

Type IVa *and IVb reinforced* embankment

Rockfall protection embankments with geosynthetics can be made slimmer and with steeper slopes. The requirements for geosynthetics are summarised in tables 3 and 4. For the freeboard, 1.5 times the block diameter is required for geogrid constructions with uphill slope inclinations of ≤ 70°. For embankments with a slope inclination of ≥ 70°, the freeboard can be reduced to the simple design block diameter D.

For embankments reinforced with geosynthetics, the ultimate limit state ULS without rockfall event and the ultimate limit state with rockfall event must be verified. The verifications differ in the approach of the partial safety factors and the material characteristic values for the geosynthetics. The larger value of the required characteristic material resistance of the reinforcement is decisive in each case. To determine the characteristic short-term tensile strength of the reinforcement, the values given in tables 3 and 4 for the design strength $R_{B,d}$ and the design elongation stiffness J_d are to be multiplied by the reduction coefficients depending on the verification method. The design value of the elongation stiffness at 5% elongation $J_{d@5\%} = R_{B,d} / 0.05$ must be derived as a function of deformation in order to ensure the transverse distribution of the loads in the longitudinal axis of the structure. In construction practice, a spacing between layers of ≤0.8 m should be selected to maintain the bond effect (Hofmann *et al*., 2017, Hofmann *et al*., 2020 and ONR

24810, 2020). Usual installation spacing is around 0.6 m.

4. Pseudo static verification-determination of the penetration depth and the static equivalent force

The verification is based on the assumption that the static equivalent force and the overall stability represents to the dynamic impact and the energy dissipation. For the estimation of the maximum static equivalent force F_k, the static equivalent force can be given by equation (1) based on the deformation energy at impact. The established basic dynamic equations (Hofmann & Mölk, 2012, Hofmann *et al.*, 2017, Hofmann *et al.*, 2020 and ONR 24810, 2020) combine the impact time t, the penetration depth δ, the velocity v, the deceleration a and the mass of the block m. Initially, the acceleration (deceleration) increases almost linearly and then decreases almost linearly. The assumed acceleration curve is shown in Figure 6. The resulting velocity curve is shown in Figure 7. The maximum deceleration, from which the static equivalent force results, can be estimated with Figure 7. The penetration depth δ is determined via the dimensionless diagram (Fig. 8). The static equi-

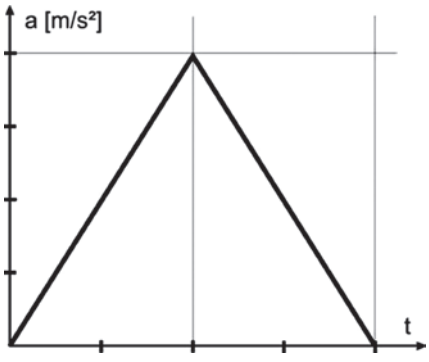

Fig. 6 – Assumed development of acceleration over time.

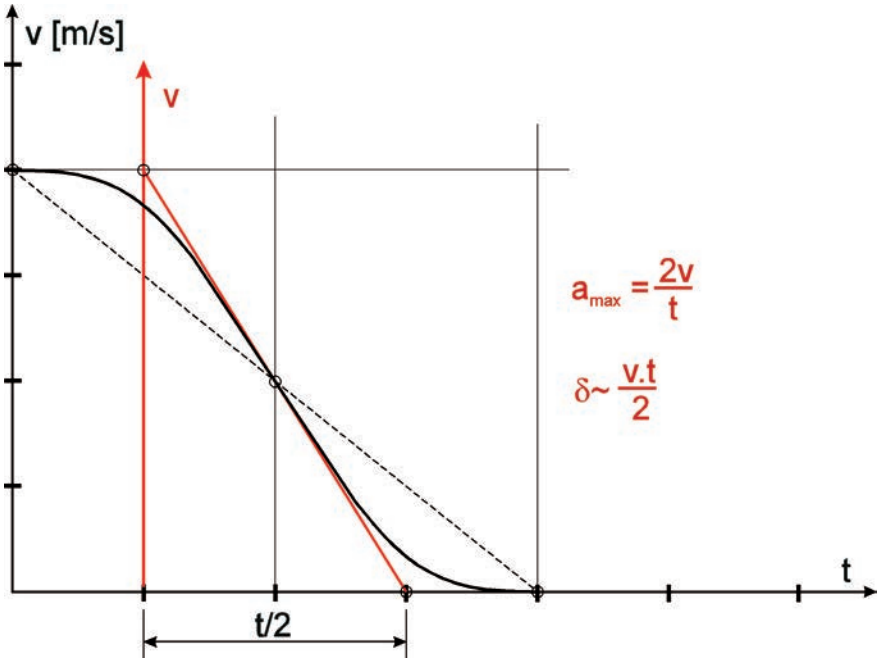

Fig. 7 – Resulting development of velocity over time.

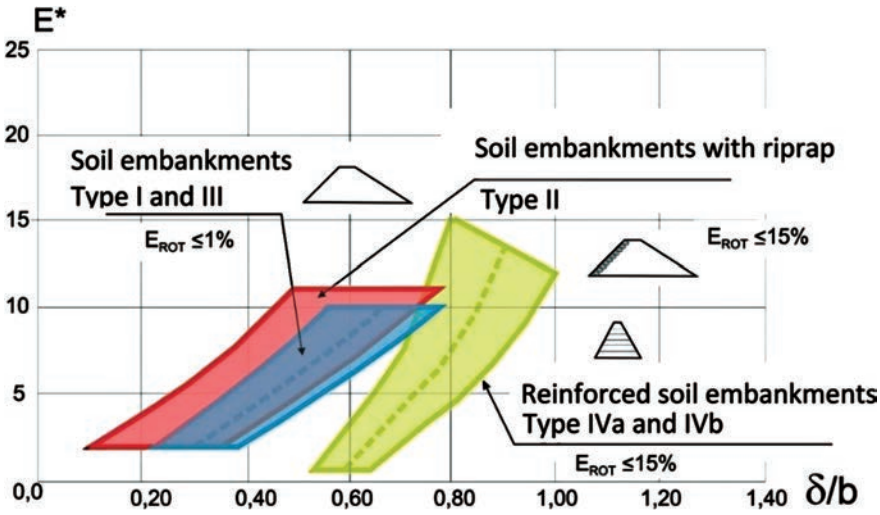

Fig. 8 – Diagram for the estimation of the penetration for rock-fall embankments (Types I, II, III, IV a and b) according to Hofmann & Mölk, 2012 for a maximum rotational energy percentage of 1% for type I and 15% for type II, III, IVa and IVb – *E** with formula (8).

$E = m\, v^2 / 2$	(joules)	(9)
m mass of the sphere	(kg)	
v velocity of the impact block	(m/s)	
$\gamma = \rho\, g$	(Nm^{-3})	
ρ density of the soil	(kg/m^3)	
g acceleration due to gravity	(m/s^2)	
$A_a = (b+c)/2\ h_a$ related embankment area	(m^2)	(10)
D impact block diameter	(m)	
h_a referred height	(m)	
b crown width	(m)	
c embankment width at height of h_a	(m)	
δ penetration depth of the sphere into the embankment	(m)	

valent force can subsequently be distributed over the activated embankments width. For each construction type, extensive model tests were performed to determine the activated embankments width. The model tests were carried out with soils without grain sizes < 0.063 mm and with a small proportion of grain sizes < 0.063 mm. No significant differences could be derived for the Impact load case.

The maximum acceleration a can be determined according to Figure 7 with formula (2). Comparisons of different models for estimating a static equivalent force (Kister & Fontana, 2015) show that the static equivalent force, with the penetration depth determined from Fig. 8 and formula (1), represents approximately an average value.

$$F_k = \frac{v^2 m}{\delta} \quad (1)$$

$$a_{max} = \frac{2v}{t} \quad (2)$$

With $$F = a_{max} m \quad (3)$$

and $$t = \frac{2\delta}{v} \quad (4)$$

$$a_{max} = \frac{v^2}{\delta} \quad (5)$$

From diagrams in which the impact force is shown over the impact time (Hübl & Nagl, 2016 and Blovsky, 2002), it can be deduced that the energie that is converted into heat during impact is approximately equal to half the product of the maximum impact force and the penetration depth. Equating the kinetic energy of the body when it hits the embankments surface and the energy that is converted into heat during deceleration yields to:

$$E_k = \frac{v^2 \times m}{2} = \int F(\delta) d\delta = \frac{F_k \times \delta}{2} \quad (6)$$

The formulae (1) and (6) agree that the static equivalent force (= the maximum impact force) is equal to

$$F_k = \frac{v^2 \times m}{\delta} \quad (7)$$

In the verification model, the impact energy is first referenced to a reference surface with a horizontal plane. The height of the referenced embankment section A_a serves as an indicator for the contributing mass. The decisive parameters for the penetration depth of the impact body into the embankment are the reference height h_a (height of the lower edge of the impact body to the embankment crown) and the crown width b.

The dimensionless reference energy E^* in Figure 8 is defined as follows according to Hofmann & Mölk, 2012:

$$E^* = \frac{E}{\gamma A_a D h a} (-) \quad (8)$$

E^* is the kinetic energy of the impacting body related to the weight of the embankment above the lower edge of the sphere (γA_a) multiplied by the sphere diameter D multiplied by the height from the lower edge of the sphere to the top of the embankment h_a (Fig. 9).

In a 1:1 experiment with a 4.8 m high dam, a crown width of 1.5 m and an inclination of the slopes of 65° (Fig. 10), a loading test with 7000 kJ was carried out (Hofmann *et al*., 2017). Based on the geometry of the embankment and the impact block energy of 7000 kJ, formula (8) results in E^* = 8.5. From the diagram Fig. 8, for type III, a δ/b 0.6 results and thus a δ = 1.5 × 0.6 = 0.9 m. For comparison,

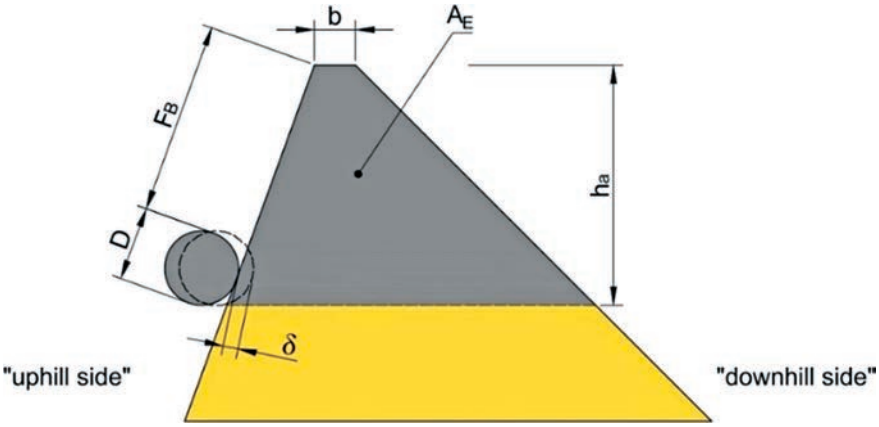

Fig. 9 – Cross section of the embankment.

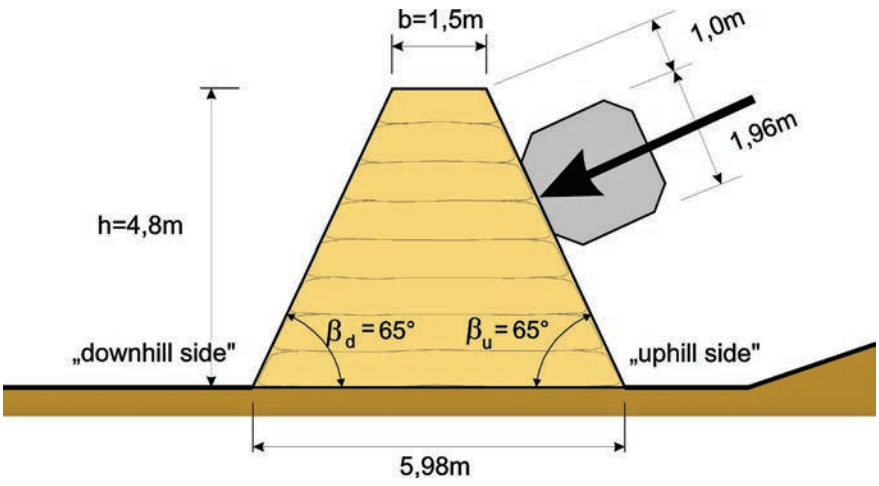

Fig. 10 – 1:1 test with rockfall protection embankment.

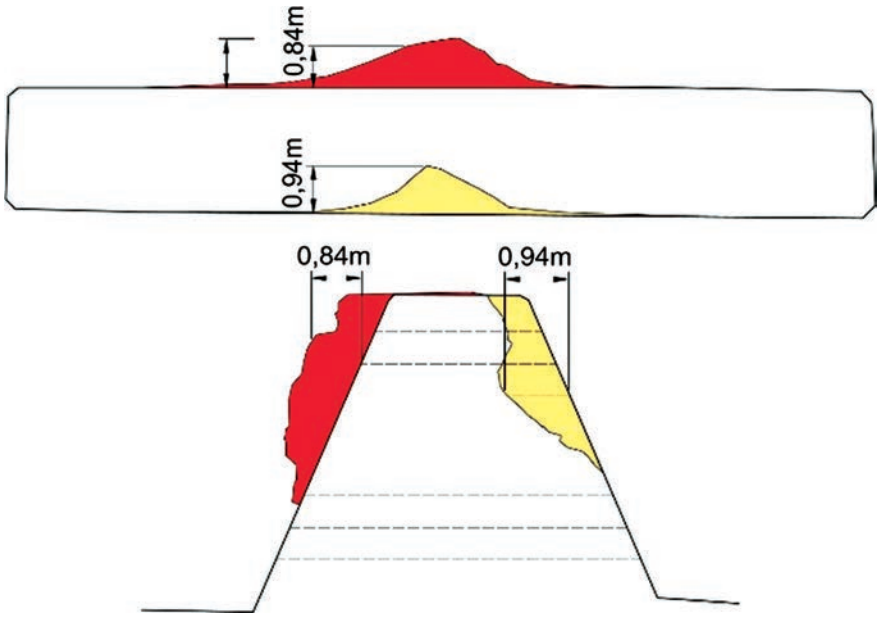

Fig. 11 – Displacements after the impact. Top ground plan, bottom cross section.

a maximum penetration depth of δ = 0.94 m was found in the 1:1 test. For the transverse distribution and the penetration depth, very good agreement was achieved with the design concept according to Hofmann & Mölk, 2012 (Fig. 11).

5. Geotechnical model for the verification

During the impact, the rotating block hits the uphill surface. The plastic displacements in the embankment cross-section have the direction of the impact block. The reinforcement is activated during the impact and prevents failure on the inclined sliding surface. The impact force is dissipated in the activated embankment body. The reinforcement confines the embankment material through the wrap around reinforcement construction and prevents mass loss or "shooting out" of the material of the embankment. The wrap around reinforcement construction results in a resisting body within the dam construction. The longitudinal reinforcement improves the mobilized dam section and the ductility of the structure.

The block's share of rotational energy is converted into translational energy by friction with the embankment surface, the block performs an S-shaped movement over the embankment crest. Therefore, the rotation of the block cannot be neglected. The more tensile the reinforcement, the smaller the width of the supporting effect of the embankment in the longitudinal axis of the embankment.

In the geotechnical verification with a stability analysis (e.g. sliding block, statics of rigid body), the static equivalent force calculated for the impact may then be distributed over the interacting embankment length (Fig. 12 right). This assumes that the soil is enclosed in a wrap around reinforcement construction and that its mass can fully participate. The decisive factor for the computational verification with rigid bodies is a slip surface approximately in the impact direction. The position of the slip surface in the embankment due to the impact as well as the size of the activated dam body could be documented with the PIV method (Particle Image Velocimetry) (Hofmann *et al*., 2017).

Table 6 compares the two verification approaches for rockfall protection embankment according to Mongiovi, (2014), Peila *et al*., (2007) and Ronco *et al*., (2009) as well as Hofmann & Mölk (2012) using the example of an embankment from Marchelli & Deangeli, 2022. Whereas for the first method (design approach) a serviceability limit state SLS design is carried out (Fig. 12 left), for the method according to Hofmann & Mölk (2012) the ultimate limit state ULS design (Fig. 12 right) has to be verified. Accordingly, the required verifications are also required for the geosynthetics. The comparison with the 1:1 test in section 4, with an energy of 7000 kJ, an embankment height of 4.8 m, a crown width of 1.5 and embankment slopes of 65° shows comparable results (Fig. 11).

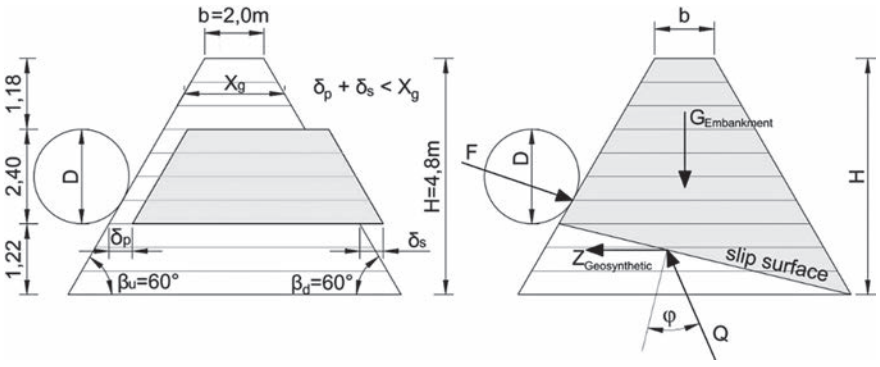

Fig. 12 – (left) Serviceability limit state verification; (right) verification of the ultimate limit state.

Tab. 6 – Comparison of the two detection methods.

Parameter		Mongiovi, L., (2014), Peila *et al*. (2007), Ronco *et al*. (2009) and Marchelli & Deangeli, (2022)	Hofmann & Mölk, (2012) and ONR 24810, (2020)
Embankment height	H	4,8 m	
Crest width	b	2,0 m	
Uphill face slope angle	β_u	60°	
Downhill face slope angle	β_d	60°	
Internal friction angle	ϕ	30°	
Impact kinetic energy	$E_k = E_d$	6.107 kJ	
Energy dissipated by friction	E_f	581 kJ	-
Energy dissipated by compacting	E_p	5.527 kJ	6.107 kJ
Force dissipated by friction	F_f	1.698 kN	-
Force dissipated by compacting	F_p	12.048 kN	15.268kN
Displacement	δ_P	0,92 m	0,74-0,80 m
Displacement	δ_S	0,68 m	-
Verification for the embankment (SLS/ULS)		Serviceability limit state $\delta_P + \delta_S = 1{,}60\ m < X_g = 1{,}68\ m$	Ultimate limit state with verification of the geosynthetics

6. Innovative construction methods

The robustness and reliability of rockfall protection embankment pose a challenge to the designers. De Biagi *et al*, 2020 and Marchelli *et al*, 2021 have already addressed this issue. De Biagi *et al*., 2020, describe the uncertainties in determining the energy and the bounce height of the impact block and give a proposal for determining the design parameters based on a semi-probabilistic framework. Marchelli *et al*., 2021 explain in their paper a time-dependent reliability approach for the impacting block to evaluate the partial safety factor for the jump height and the energy. The design value of the jump height and the energy of the impact block were the two essential parameters for the design of the construction and the sustainability of an innovative construction method.

Figure 13 shows a 167-layer, 67 cm thick, geogrid-reinforced protective embankment, type IVa, over a height of 104 m on slope inclination at 35-38°, next to the crest of a 160 m high dam in the Kaunertal valley. The 20 m high protective embankment with a crown width of 5.0 m and slopes of 70° was built as a rockfall protection embankment and as a protective structure against an rock avalanche. The facing on the uphill slope of the embankment was made with larch wood (Fig. 13 to 15). The spacing between

Fig. 13 – Example for geotextile-reinforced construction of type IVa embankment.

Fig. 14 – Example for geotextile-reinforced construction of type IVa with facing made of larch wood

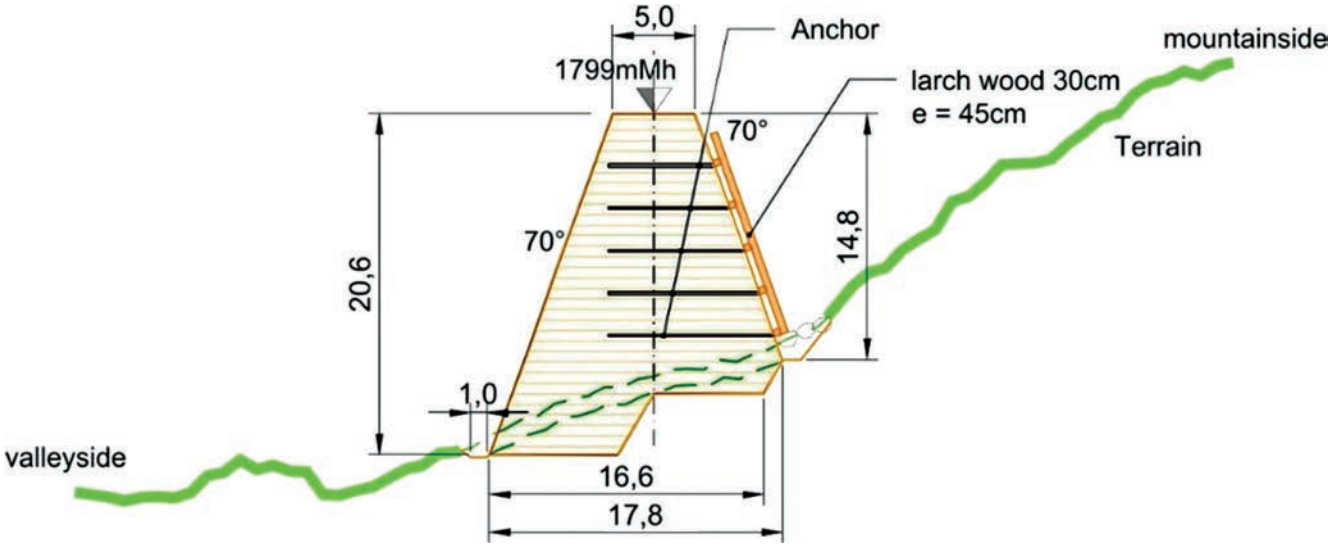

Fig. 15 – Cross-section of dam according to type IVa (Kaunertal) with facing made of larch wood.

the 30 cm thick tree trunks is 45 cm. This facing to protect the geogrids in case of smaller rockfalls could be carried out in a short construction time before winter. First events confirm the effect of the protection of the surface. Easy repair after an event is the great advantage of this construction.

Rockfall events inevitably lead to damage and wear of the surface of the uphill slope. The top layer of the slope should therefore, as far as possible, effectively protect the substance of the reinforced structure, require little maintenance and ideally be repairable so that partial damage can be repaired.

Stone facing, but also gabion constructions, can greatly limit the superficial damage to the supporting embankment through sufficient robustness. The protective layer and its individual elements should be designed for the expected stresses. For mechanical damage due to rockfall, appropriate rehabilitation plans should be provided for the front.

Figure 16 shows an example of a slender gabion solution that is repairable and can be constructed independently. Due to the double-shell design with separation between the static load-bearing system and the outer skin, the construction can be made slimmer than classic gabions and is thus often economically interesting in addition to the technical advantages. Figure 17 shows a variant with a damping wear layer made of used tires.

Figure 18 and 19 shows a type IVb dam structure with longitudinal reinforcement and a combined protection and foundation measure for high impact energy. The embankment structure was founded on a very steep slope using bored piles. To increase the usable height, a rockfall protection net was founded on the embankment structure with micropiles.

Fig. 16 – Reparable facing (half-gabion) as protection of the static construction executed in folded-method (pictues: NAUE GmbH&Co KG), damaged facing after rock-fall (left), installation of new facing (centre), new filling (right) (Hofmann & Vollmert, 2020).

Fig. 17 – Deposition zone of a rock-fall embankment with facing made of used car-tires (pictues: NAUE GmbH&Co KG) (Hofmann & Vollmert, 2020).

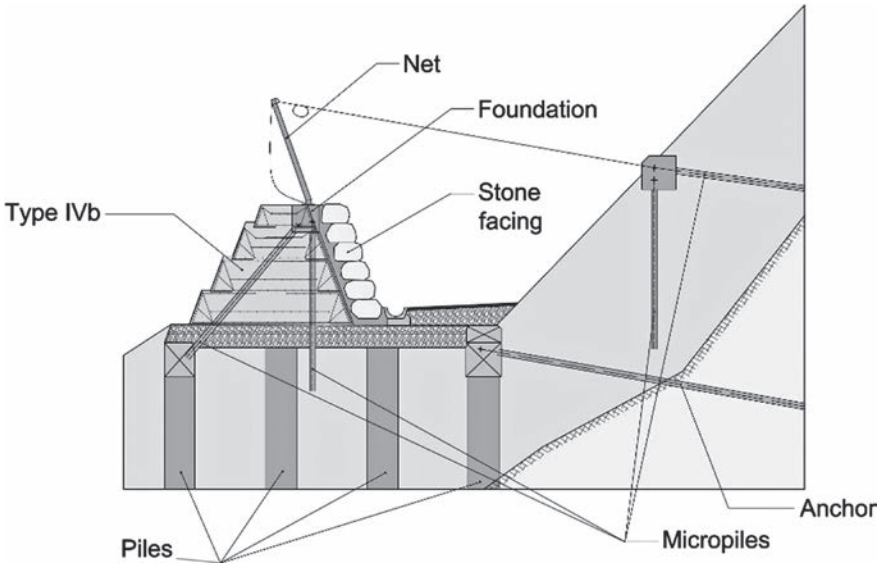

Fig. 18 – Example of a dam with combined protection and foundation measures with longitudinal reinforcement according to type IVb.

7. Summary

Various models are available for the design of rockfall protection embankment. This paper presens a "rheological model" in combination with the computational determination of the acting force (Peila *et al*., 2007, Ronco *et al*., 2009) as well as the method of Hofmann & Mölk, (2012). While the method according to Peila *et al*., (2007) and Ronco *et al*., (2009) considers the proof of the protective embankment via the path of permissible displacements of the local dam body, i.e. the serviceability SLS, the method according to Hofmann & Mölk, (2012) considers the proof via the ultimate limit state ULS. In the latter calculation model, different types of structures (embankment with stone facing, reinforced structures and embankments without geosynthetics) can be taken into account. The observed and documented stresses of rockfall protection embankments after an impact confirm the model based on the depth of penetration. For both methods, additional 1:1 tests with the different construction types are required for validation.

The research was carried out with geogrids with different tensile strengths and extensional stiffnesses and the minimum requirements for the three construction types III, IVa and IVb were deri-

Fig. 19 – Example of a dam with combined protection and foundation measures with longitudinal reinforcement according to type IVb (Kunz & Jost, 2019).

ved. The differentiation into construction types for different design energies should enable a more economical, sustainable and robust construction method with high reliability. In the research work with model experiments, the failure mechanism due to rockfall as well as the transverse distribution (the activated dam section) of the impact was mapped for the construction types. The experiments with the different model soils (soil without grain sizes < 0.063 mm and soils with a small proportion of grain sizes < 0.063 mm), on the other hand, did not lead to any necessary adjustment of the design concept. The PIV method (Particle Image Velocimetry) was used to determine the activated fracture body and to verify the transverse distribution. A significant confirmation of the design diagram (Fig. 8) was the evaluation of a test with a 1:1 prototype (Fig.10).

To increase the robustness and reliability of rockfall protection embankments, innovative constructions are essential. In this paper, innovative embankments with different facings (gabions, riprap, car tires and wooden logs) were presented to protect the surface of the embankments with geogrids in case of impacts with lower energies. Through a sustainable front formation, ongoing remediation can be minimized.

References

Office for Forests of the Canton of Bern, Natural Hazards Division: Projektierung von Steinschlagschutzdämmen.

Einwirkungen infolge Steinschlags auf Schutzgalerien, (2008). ASTRA Bundesamt für Straßen.

Blovsky, S., (2002). Reinforcement possibilities with geosynthetics. Dissertation. Vienna University of Technology. Institute for Foundation Engineering and Soil Mechanics.

De Biagi, V., Marchelli, M., & Peila, D, (2020). Reliability analysis and partial safety factors approach for rockfall protection structures. Engineering Structures, 213, 110553.

Hofmann, R., Mölk, M., (2012). Design proposal for protective dams. Geotechnik 35, H. 1, pp. 22-33.

Hofmann, R., Vollmert, L., Mölk, M., (2013). Rockfall-protection embankments – design concept and construction details. Proceedings of the 18th International Conference on Soil Mechanics and Geotechnical Engineering, Paris 2013.

Hofmann, R., Mölk, M., Vollmert, L., (2017). Rockfall protection dams – Design proposal for different construction types. geotechnik 40, H. 1, pp. 35-53.

Hofmann, R., Vollmert, L., (2020). Rockfall embankments: Construction and Design. Geomechanics and Tunnelling 13, No. 1. DOI: 10.1002/geot.201900073.

Hübl, H., Nagl, G., (2016). Rockfall on steel snow bridge. University of Natural Resources and Applied Life Sciences. Institute for Alpine Natural Hazards. Report Unpublished.

Kister, B., Fontana, O., (2012). On the uncertainties in the determination of input parameters for the design of rockfall protection dams. 8 th Colloquium Bauen in Boden und Fels, Technical Academy Esslingen, 17 and 18 February 2012. Proceedings, pp. 241-254.

Kretz, A., (2018). Rockfall protection dams – Proposal and comparison of a rheological design model. Swiss Bulletin of Applied Geology. Vol. 23/2.

Kunz, L., Jost, S., (2019). Protection against gravitational natural hazards with innovative earthworks technology, CH-Weggis. Proceedings of the NAUE Geosynthetics Colloquium.

Marchelli, M., De Biagi, V., & Peila, D., (2021). Reliability-based design of rockfall passive systems height. International Journal of Rock Mechanics and Mining Sciences, 139, 104664.

Marchelli, M., Deangeli, C., (2022). Towards a codified design procedure for rockfall reinforced earth embankments. GEAM, Geoingegneria e attività estrattiva.

Mongiovi, L., Bighignoli, M., Danzi, A., Recalcati, P., (2014). An impact test on a reinforced earth embankment. Proceedings of Interdisciplinary workshop on rockfall protection – Rocexs 2014, Lecco, Italy.

ONR 24810, (2020). Technical protection against rockfall – Terms and definitions, effects of actions, design, monitoring and maintenance. *Austrian Standards Institute.*

Peila, D., Oggeri, C., & Castiglia, C., (2007). Ground reinforced embankments for rockfall protection: Design and evaluation of full scale tests.Landslides, vol. 4, n. 3, pp. 255-265.

Ronco, C., Oggeri, C., Peila, D., (2009). Design of reinforced ground embankments used for rockfall protection. Natural hazards and earth system sciences 9, 1189-1199.

Development of principles for the design of rockfall protection dams, (2015). Swiss Confederation. Federal Department of the Environment, Transport, Energy and Communications DETEC, Federal Roads Office.